Journal of Crystal Growth 65 (1983) 324–330
North-Holland, Amsterdam

PLASTIC DEFORMATION INFLUENCE ON STRESS GENERATED DURING SILICON SHEET GROWTH AT HIGH SPEEDS

J.C. LAMBROPOULOS and J.W. HUTCHINSON

Division of Applied Sciences, Harvard University, Cambridge, Massachusetts 02138, USA

and

R.O. BELL, B. CHALMERS and J.P. KALEJS

Mobil Solar Energy Corporation, Waltham, Massachusetts 02254, USA

Plastic deformation processes have been studied in high speed silicon sheet growth using finite element analysis. Stress and strain rate distributions are calculated for steady-state growth of thin sheet under plane stress conditions. Predictions of the model are used to examine factors affecting residual stress and buckle formation for growth of silicon ribbon by the EFG method.

1. Introduction

A satisfactory model that can account for stresses arising during growth of silicon sheet at high speeds is not yet available. Stresses generated in growth of silicon ribbon by the EFG technique can lead to buckling and residual stresses large enough to make thin ribbon (≤ 300 μm) unsuitable for fabrication into solar cells [1]. Previous attempts to calculate stress distributions for silicon sheet grown by various techniques have had limited success in predicting stress distributions for realistic growth conditions [2,3]. Simple thermoelastic theory shows that temperature distributions exist that allow growth of sheet for which all points remain in a state of zero stress. However, these conditions have not been achieved for sheet growth techniques that require high temperature gradients (≥ 1000°C/cm) in the solid near the growth interface in order to sustain high speed growth (≥ 3 cm/min). All efforts to model stresses have failed to include plastic deformation effects. Their impact on the stress distribution in the sheet is thus not understood.

This paper describes a finite element modeling approach that can fully take into account plastic deformation effects on the stress distribution setup in a sheet grown at high speeds under steady-state conditions. The model and theoretical considerations are discussed in section 2. The method has been applied in a preliminary study to obtain stress distributions for growth of EFG silicon ribbon. Results and discussion of the modeling are presented in sections 3 and 4. These illustrate, on a qualitative level, the impact that plastic deformation processes may have on residual and buckling stresses in silicon sheet grown at high speeds. The aspects of the physical model that are required to take the calculations beyond a qualitative level are examined in section 5. The broader implications of the method will be explored in a later paper.

2. Model for stress calculation

The computer code developed for analyzing the stress distribution in a ribbon pulled from the melt through an arbitrary temperature field is similar to methods used to study steady-state crack growth problems in elastic–plastic and in elastic–creeping solids [4]. A ribbon of width $2H$, extending from $y = -H$ to $y = +H$, emerges from the melt at $x = 0$ and is pulled in the positive x-direction with uniform velocity V. The temperature distribution

0022-0248/83/$03.00

in the ribbon, $T(x, y)$, is assumed to be independent of time. The sheet modeled is of half-width $H = 4$ cm and length $L = 20$ cm. The ribbon end at $x = 20$ cm is at room temperature. The sheet length must be chosen so that over a sufficiently large portion of the cold end the temperature profile is linear. This ensures that the residual stresses calculated at the cold end are the same as those at room temperature. Temperature uniformity in the y-direction is assumed for this initial study. The grid pattern used in the calculations has a nonuniform mesh which is made very fine close to the growth interface to provide high resolution for the stress calculation.

Plane stress conditions are assumed, with nonzero stresses σ_{xx}, σ_{yy} and σ_{xy}. For steady-state growth, the stresses, strain rates and velocities are independent of time at any spatial point (but not for a material element). With V the overall pull velocity, additional material velocity components in the x- and y-directions are denoted by v_x and v_y, respectively, so that the total velocity components are $V + v_x$ and v_y. The strain rates are then $\dot{\epsilon}_{ij} = \frac{1}{2}(v_{i,j} + v_{j,i})$.

The silicon is taken to be an elastic–creeping solid with a constitutive law of the form:

$$\dot{\epsilon}_{ij} = \frac{1+\nu}{E}\dot{\sigma}_{ij} - \frac{\nu}{E}\dot{\sigma}_{kk}\delta_{ij} + \dot{\epsilon}^{c}_{ij} + \alpha\dot{T}\delta_{ij}. \tag{1}$$

The material constants used for silicon are $\nu = 0.3$, $E = 165$ GPa and a thermal expansion coefficient [3]

$$\alpha = 2.552 \times 10^{-6} + 1.95 \times 10^{-9}T - 9.0 \times 10^{-15}T^2.$$

Additionally, for steady-state $\dot{T} = V(\partial T/\partial x)$. The creep contribution $\dot{\epsilon}^{c}_{ij}$ modeled is of the form

$$\dot{\epsilon}^{c}_{ij} = C\left[\exp(-\beta/T)/T\right](\sigma_e/\mu)^{n-1}S_{ij}, \tag{2}$$

where $\mu = 63.7$ GPa is the elastic shear modulus, S_{ij} is the deviatoric part of the stress, and

$$\sigma_e = \sqrt{\tfrac{3}{2}S_{ij}S_{ij}}$$

is the effective stress. A primary creep term is not included in eq. (1). In principle, more accurate creep descriptions can be modeled; however, the available data for silicon do not appear to justify a more complicated description at this point.

In addition to the above equations, the equations of in-plane equilibrium, $\dot{\sigma}_{ij,j} = 0$, must be specified. The equivalent variational equation of equilibrium is:

$$\int_A \dot{\sigma}_{ij}\delta v_{i,j}\,\mathrm{d}A = 0, \tag{3}$$

and no boundary terms are involved since the tractions vanish everywhere on the boundary. The stress-rate field is related to the stress field by the steady-state equation

$$\dot{\sigma}_{ij} = V(\partial\sigma_{ij}/\partial x).$$

Assuming that all stresses are zero at the melt interface (discussed further below), this implies:

$$\sigma_{ij} = V^{-1}\int_0^x \dot{\sigma}_{ij}\,\mathrm{d}x. \tag{4}$$

The numerical method uses a velocity-based finite element method to discretize the fields. The problem is inherently nonlinear and therefore an iterative procedure is employed to obtain the solution. The iterative scheme works as follows. At the end of any iteration, stress and creep strain rate values are available in each element for use in the next iteration. A finite element method, that uses a variational formulation incorporating both creep strain and thermal strain rates as body force terms, is used to obtain an improved estimate of the velocity field. From the velocities, a new estimate of the total strain-rate is computed, and, through eq. (1), the stress-rate is available. Finally, stresses are recalculated from eq. (4) to complete the iteration.

The method described above has been applied to calculate stress and strain distributions for the two sheet temperature profiles given in fig. 1 in order to illustrate plastic deformation manifestations in silicon sheet growth. Profile 1 is representative of a temperature distribution in a 300 μm thick ribbon growing in an EFG cartridge system developed for growth of 10 cm wide ribbon. Cooling elements are located about 0.1 cm from the interface to enhance the speed capability, and an active afterheater is placed 1 cm from the

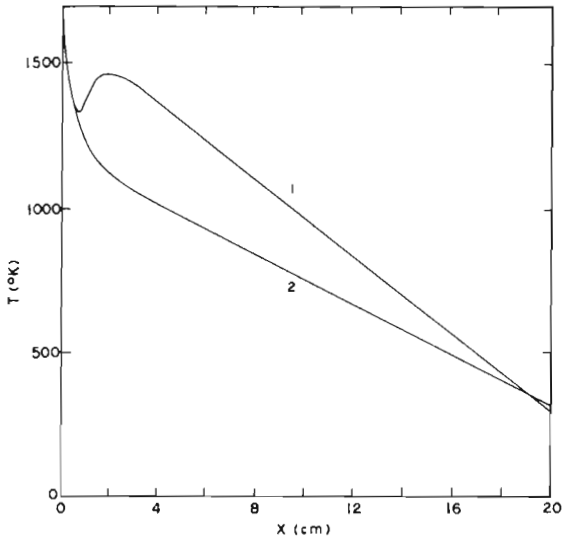

Fig. 1. Temperature profiles along growth direction used in modeling of sheet stresses: (1) EFG system; (2) idealized system.

interface for annealing purposes. This profile has been obtained from a combination of experimental data and detailed heat transport modeling, as described elsewhere [5]. The second profile studied, curve 2 of fig. 1, is derived in part from the experimental profile: Both profiles are identical between the growth interface and about 0.4 cm; thereafter this second profile has no reheat region but gradually turns into a linear profile beyond about 2 cm from the interface.

Complicated creep behavior has been reported at high ($\geq 1000°C$) temperatures in silicon [6,7]. A creep law expression of the form of eq. (2) valid for all stress levels and temperatures is not found. β is reported to be temperature dependent and exponents, n, ranging from 2 to 11 have been observed. Since creep behavior appropriate to high speed sheet growth conditions has not been investigated, we have chosen to model steady-state creep with a stress dependence of $n = 5$, and $\beta =$

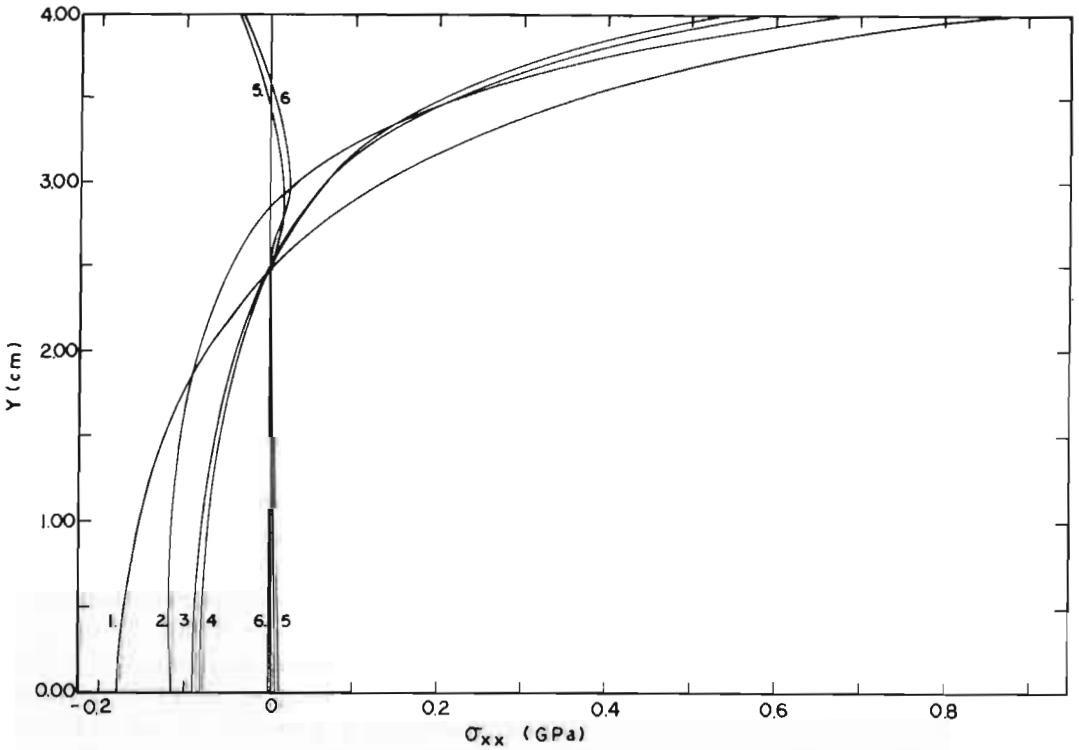

Fig. 2. σ_{xx} variation across the sheet width at $x = 20$ cm (room temperature) for the high creep case. Elastic solutions for (1) idealized system and (2) EFG system are compared to the solid with creep: idealized system: (3) at $V = 3$ cm/min and (4) at $V = 6$ cm/min; EFG system: (5) at $V = 3$ cm/min and (6) at $V = 6$ cm/min.

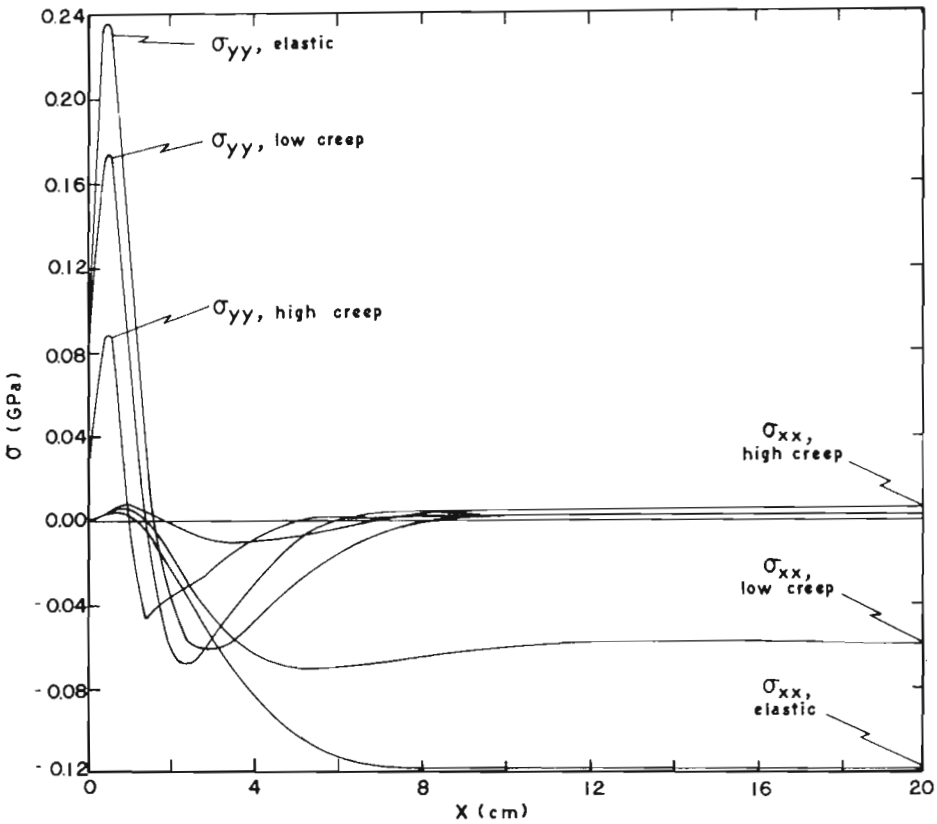

Fig. 3. σ_{xx} and σ_{yy} variations along growth direction near ribbon centerline ($y/H = 0.025$) for EFG system at $V = 6$ cm/min.

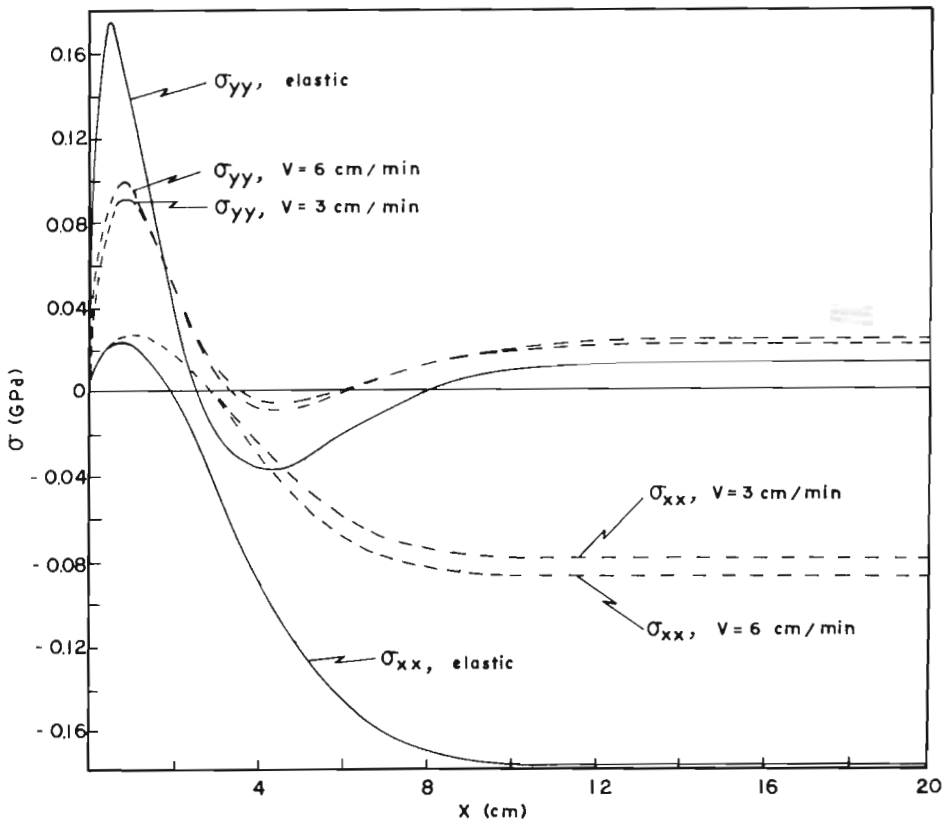

Fig. 4. σ_{xx} and σ_{yy} variations along growth direction near ribbon centerline ($y/H = 0.031$) for idealized system and high creep condition.

5.976×10^4 K, representative of intermediate stress level creep with an activation energy typical of self-diffusion. The constant C is fixed at 1.05×10^{29} K/s · GPa by a fit of creep data at 1300 K in one case (the "low creep" condition) [6]; a second case with C increased by a factor of 10^2 is also examined (the "high creep" condition). The choices made for a representative creep relation for the modeling do not appear to invalidate an examination of plastic deformation processes at the intended qualitative level of the discussion that follows.

3. Results

Comparisons of stress distributions for growth of an elastic sheet with a solid capable of creep according to eq. (2) are given in figs. 2 to 4. Fig. 2 gives the variation of the stress component σ_{xx} (residual stress) across the sheet width at room temperature ($x = 20$ cm). Solutions at growth speeds of 3 and 6 cm/min are given here for high creep conditions. Distributions for σ_{xx} and σ_{yy} in an elastic solid near the sheet center line for the cartridge system are compared in fig. 3 to those for the two creep conditions at $V = 6$ cm/min. In fig. 4, the variation of the stress components σ_{xx} and σ_{yy} with growth speed for the high creep condition is given over the length of the sheet near the center line for the idealized profile of fig. 1. Strain-rate component distributions along the sheet center line are given under high creep conditions for the two temperature distributions in fig. 5.

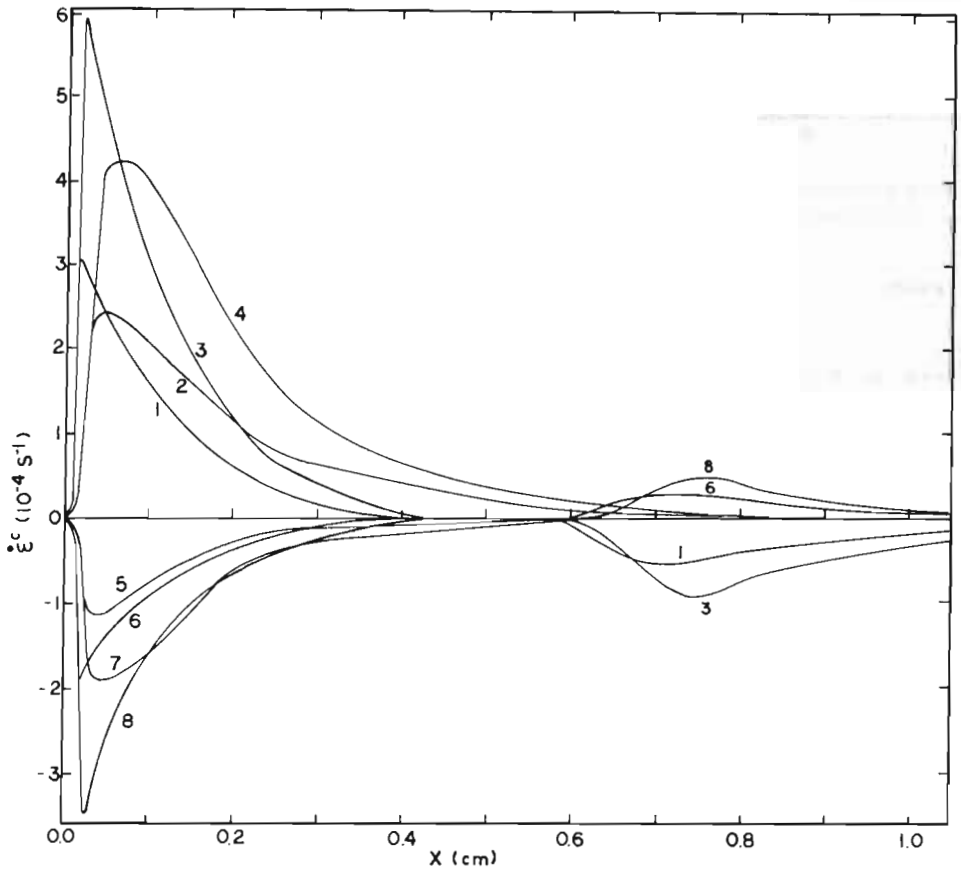

Fig. 5. Creep strain rate variations along growth direction near ribbon centerline for high creep conditions: (1), (3) $\dot{\epsilon}^c_{yy}$ for EFG system at 3 and 6 cm/min; (2), (4) $\dot{\epsilon}^c_{yy}$ for idealized system at 3 and 6 cm/min; (5), (7) $\dot{\epsilon}^c_{xx}$ for idealized system at 3 and 6 cm/min; (6), (8) $\dot{\epsilon}^c_{xx}$ for EFG system at 3 and 6 cm/min.

4. Discussion

The calculated distributions in figs. 2 to 4 show that the extent to which stresses are reduced by creep from those in an elastic solid is particularly sensitive to details of the temperature profile in the sheet. In the range of growth speeds considered, variation of peak σ_{xx} and σ_{yy} values with speed is less than that produced by the hundredfold change in the creep both in the low and high temperature regions. The creep strain rate varies proportionally to growth speed (fig. 5). This dependence on speed is considerably stronger than that for σ_{xx} and σ_{yy}.

Experimental data are not available to provide a test for the predictions of the modeling on a quantitative level. However, some observations give insight in a number of areas that may be valuable in helping to guide future modeling directions. These come in the form of information on residual stress and buckling associated with 10 cm wide ribbon grown in the EFG system, represented by profile 1 in fig. 1. Average residual sresses in this ribbon are observed to be low, of the order of 1 MPa, as estimated at an order of magnitude level using a "split-ribbon" technique [3]. While the residual stress level does not measurably increase with speed over the range from 2.5 to 4.5 cm/min, ribbon buckling does become more severe with the increases in speed. The buckles are permanent, i.e., not elastic deformations, and appear to be essentially "frozen in" by high temperature stress relief.

Tentative conclusions that can be made from these experimental observations are:

(i) Creep rates comparable to the highest values calculated (fig. 5) are needed to reduce residual stresses from those typical of an elastic sheet to levels of the order of those observed in ribbon grown with the EFG system. At this point, the validity of the creep law of the form modeled cannot be evaluated because of other factors that influence the solutions generated (see section 5 below).

(ii) The stresses likely to cause the buckling observed in EFG ribbon are dominated by σ_{yy}, which has its peak values within 1 cm of the interface (fig. 3). For all the conditions examined, the peak values of σ_{yy} remain much greater than σ_{xx} and they do not undergo the large variations with creep intensity that are observed for the residual stress. If appreciable stress relief is to be accomplished after buckle formation near the interface with the EFG system, then creep rates typical of the high creep conditions modeled again are required.

(iii) In the absence of the annealing region provided by the active afterheater in the EFG system, i.e., for profile 2 of fig. 1, σ_{xx} can be decreased only by assumption of a higher creep rate than that modeled, or by an extension of the linear portion of the profile closer to the interface.

5. Conclusions

The effects of plastic deformation on the stress generated during high speed silicon sheet growth have been studied with the help of finite element analysis of steady-state growth. The method has been applied to calculating stress and strain rate distributions for two sheet temperature profiles. The extent to which creep reduces residual stress is shown to be very sensitive to the details of the sheet temperature profile. In the case of a temperature distribution typical of a ribbon grown with an EFG cartridge system, significant reductions of residual stress by creep are predicted to occur at growth speeds between 3 and 6 cm/min.

Quantitative application of the model is not warranted at this time. The results can only be taken as indicative of the kinds of predictions that are possible because there is a need for more detailed information in several areas. The mathematics of the steady-state model used here is such that any interface stress distribution $\sigma_{yy}(y)$ may be specified. The value σ_{yy} may take on at the interface depends upon the physics of the solidification process. This is not known for the high speed sheet growth mode examined, and a value of $\sigma_{yy} = 0$ has been used for model illustration purposes. Finally, the creep response of the sheet to the type of stresses that arise very near the interface needs to be identified to permit choice of an appropriate constitutive relation for plastic deformation processes.

Acknowledgements

This paper is based on work sponsored by the Jet Propulsion Laboratory, California Institute of Technology, under Subcontract No. 956312 and is part of the Advanced Materials Research Task of the US DOE Flat Plate Solar Array Project.

Note added in proof

Support for use of creep intensities even higher than the "high creep" condition modeled here is recently available from the experimental work of Siethoff and Schröter [8].

References

[1] J.P. Kalejs, B.H. Mackintosh and T. Surek, J. Crystal Growth 50 (1980) 175.
[2] R.W. Gurtler, J. Crystal Growth 50 (1980) 69.
[3] R.G. Seidensticker and R.H. Hopkins, J. Crystal Growth 50 (1980) 221.
[4] R.H. Dean and J.W. Hutchinson, Fracture Mechanics,, ASTM-STP 700 (American Society for Testing and Materials, Philadelphia, PA, 1980) p. 383.
[5] J.P. Kalejs et al., First Quarterly Report, DOE/JPL 956312/82/01 (October, 1982) (unpublished).
[6] M.M Myshlyaev, V.I. Nikitenko and V.I. Nesterenko, Phys. Status Solidi 36 (1969) 89.
[7] H.J. Frost and M.F. Ashby, Deformation Mechanism Maps for Ceramics, Cambridge University Publication CUED/C/MATS/TR.79, May 1981.
[8] H. Siethoff and W. Schröter, Scripta Met. 17 (1983) 393.